Supporting Information: How to Dope the Basal Plane of 2H-MoS_2 to Boost the Hydrogen Evolution Reaction?

Nawras Abidi,[†] Audrey Bonduelle-Skrzypczak,[‡] and Stephan N. Steinmann*,[†]

†*Univ Lyon, Ens de Lyon, CNRS UMR 5182, Laboratoire de Chimie, F69342, Lyon, France*

‡*IFP Energies nouvelles, Rond-point de l'échangeur de Solaize, 69360 Solaize, France*

E-mail: stephan.steinmann@ens-lyon.fr

Phone: (+33)4 72 72 81 55

Contents

S1 MoS_2 Nanotubes as HER catalysts?

Morphological changes, such as convex or concave surfaces, might lead to a higher intrinsic activity. As a convenient proxy for such curved surfaces, we herein study MoS_2 nanotubes. The structural, elastic and electronic properties of these nanotubes are well documented in the literature.[S1–S3] In addition, they have been explored as a medium for gas storage.[S4] However, their potential as HER catalysts has not been assessed so far.

Nanotubes are structures that are conceptually obtained when a ribbon of a two-dimensional material such as graphene or MoS_2 is rolled up into a cylinder. In the case of hexagonal 2D materials such as graphene it is customary to define two integers m and n to describe the direction of the vector along which the nanotube coils, or $n.\overrightarrow{e_1} + m.\overrightarrow{e_2}$. As a consequence of this definition, when $m = 0$, the nanotube has a "zigzag" like structure, in the sense that the "edges" (or limits of the unit cell) of the nanotube resemble the zigzag edge of the corresponding nanoribbon. When $m = n$, the nanotube has an "armchair" type structure, following the same analogy with graphene edges. For other combinations of m and n the nanotube is chiral. These edge configurations determine many of the material properties, especially electrical conductivity. The same concept is also applied in the case of molybdenum disulphide and we obtain MoS_2 nanotubes by rolling 1H–MoS_2 monolayer onto itself. Both armchair (n,n) and zigzag (n,0) nanotube configurations are studied. (see Figure S1). The terminations of zigzag nanotube looks like a sawtooth, while in armchair, they look like a row of seats with armrests and Mo and S atoms are aligned.

For zigzag nanotubes, we used n = [8, 10, 12, 14]. The corresponding systems range from $Mo_{32}S_{64}$ to $Mo_{56}S_{112}$ and the diameters of the nanotubes are comprised between $\sim$7 Å and 12 Å. For armchair nanotubes, n = [6, 8, 10, 12, 14] have been considered. These models correspond $Mo_{46}S_{96}$ to $Mo_{112}S_{224}$ and the diameters vary from $\sim$ 9 Å to 22 Å. All these structures were built using ATK Virtual NanoLab.[S5]

For the nanotubes, various positions were tested, for example Top S, Top Mo, Bridge, Hollow, Bent and "inside".

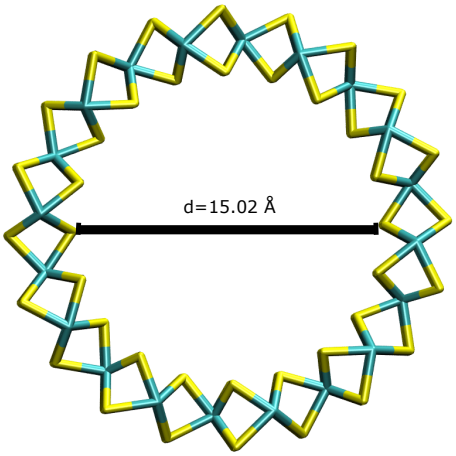

(a) (10,10) Armchair nanotube

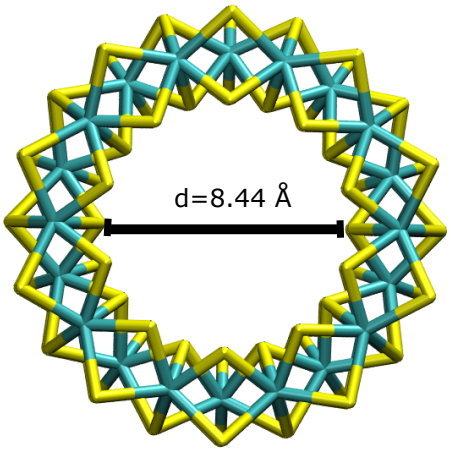

(b) (10,0) Zigzag nanotube

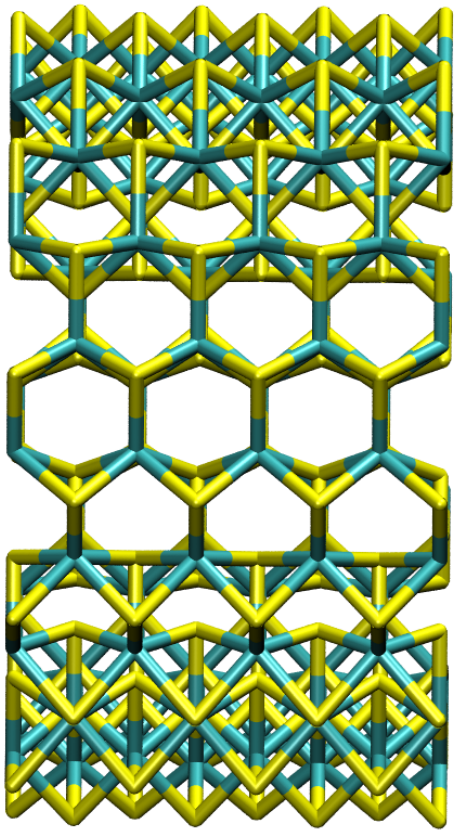

(c) (10,10) Armchair nanotube

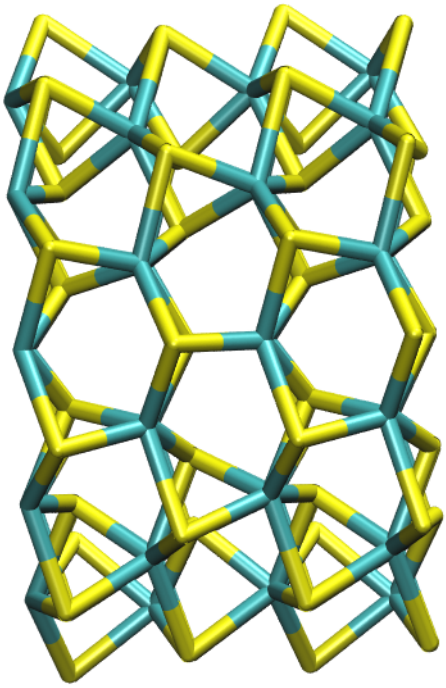

(d) (10,0) Zigzag nanotube

Figure S1: (a), (b) Cross-sectional view with the diameters of the Armchair and Zigzag nanotubes. For the same n, the Armchair diameter is bigger than the Zigzag diameter, (c), (d) Side view.

To evaluate the effect of curvature on the HER activity over MoS_2, we investigate two families of nanotubes as a function of their size. The atomic structure of the nanotubes, including cell constants, have been fully relaxed prior to H adsorption. Table S1 provides a summary of the main features (size, band-gap, relative energies) of the nanotubes, including a comparison with infinite 2D MoS_2 monolayers.

Table S1: Size, relative energies (per MoS_2 unit) and fundamental band-gap of MoS_2 mono-layers and armchair and zigzag nanotubes.

	Diameters (Å)	ΔE (eV)	Gap (eV)
Mono-layers			
1H		0.00	2.23
1T		0.69	0.24
1T′		0.45	0.42
1T″		0.52	0.37
Armchair NT			
(6,6)	8.50	1.21	0.49
(8,8)	11.73	0.76	0.87
(10,10)	15.02	0.52	1.17
(12,12)	18.46	0.38	1.33
(14,14)	21.82	0.29	1.49
Zigzag NT			
(8,0)	6.75	1.85	0.13
(10,0)	8.44	1.32	0.35
(12,0)	10.21	1.00	0.59
(14,0)	12.04	0.79	0.82

As could be expected considering the mechanical strain, the nanotubes are energetically less stable than the 1H monolayer. However, as the size increases, they become competitive with the reconstructed 1T monolayers, indicating that the (large) structures in themselves are energetically relevant. At similar diameters, the zigzag NTs are slightly ($\sim$0.1 eV per formula unit) less stable than the armchair ones, in line with previous reports.[S6] Similarly, the fundamental gap of the zigzag NTs is also a bit smaller compared to the armchair. The various 1T phases have a smaller fundamental gap than even the smallest armchair NT. In other words, while the curvature reduces the band-gap significantly with respect to the 1H monolayer, crystal-phase engineering to reach 1T-like phases seems overall more

promising to significantly decrease the band-gap.

Various positions for H adsorption have been tested both inside and outside of the NTs. The most stable adsorption mode is always located on the outside (see Table S2). Note that for the smallest NTs (6,6) and (8,0) the adsorption of H leads to the opening of the NTs, i.e., they relax to two "edge" models of MoS_2. The evolution of ΔG_H as a function of the size n of the NTs is reported on Figure S2.

Compared to the perfectly planar 1H monolayer, where $\Delta G_H \approx 1.7$ eV, the largest (and thus most stable) NTs only afford a slight activation (0.2-0.4 eV). Even for the smaller, but still stable, NTs ΔG_H drops only to about 1 eV, very far from the target range of about 0 eV. Hence, introducing curvature in MoS_2 in the absence of other activating effects is not a promising avenue towards an increase of intrinsically better active sites. Nevertheless, the curvature might be an efficient means to introduce a higher number of sulfur defects, tune the conductivity of the catalytic layer and/or exposing highly active edge sites. Indeed, experimentally much larger curved shapes have been synthesized and found to be highly active for hydrogenation reactions.[S7] However, the atomic scale origin of this increased activity has not been unraveld so far and our results demonstrate that the active sites are not the perfect basal plane of such curved morphologies.

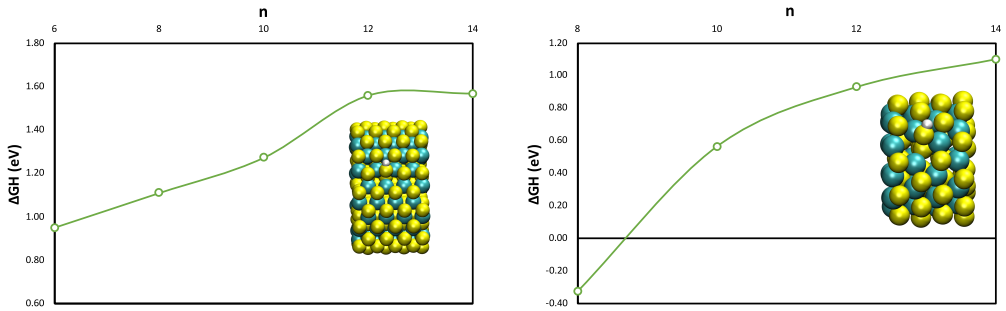

(a) Armchair (n,n) nanotube (b) Zigzag (n,0) nanotube

Figure S2: Evolution of the hydrogen adsorption energy as a function of the nanotube chiralities for (a) armchair nanotubes and (b) zigzag nanotubes.

Table S2: The hydrogen adsorption energies inside armchair and zigzag MoS_2 nanotubes for all sizes except the lowest, as the nanotube opens and becomes edges after hydrogen adsorption.

Armchair	n	Hydrogen adsorption energy (eV)
	8	1.71
	10	1.78
	12	2.10
	14	1.99
Zigzag		
	10	1.30
	12	1.40
	14	1.47

S2 Additional Figures and Tables

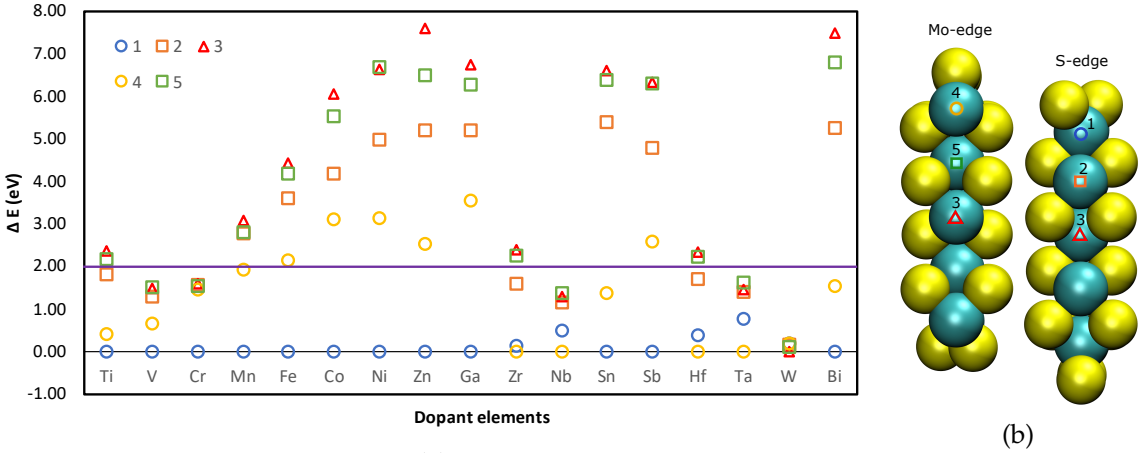

(a) (b)

Figure S3: (a) Visualization of the different elements doping the the 50%S Mo-edge and the 50%S S-edge and the energy of the structure for each position starting from 1 to 5. 1 and 2 are located at the S-edge, 4 and 5 are located at the Mo-edge and 3 refers to the basal plane. The purple line limits the range of the acceptable values for doping the basal plane. Under this value, the element can dope the basal plane of MoS_2. (b) The different positions in the 50%S Mo-edge and the 50%S S-edge for the doping elements. The circles are the edges where blue is the S edge and yellow is the Mo edge, the orange and green squares represent the second layer, and the red triangles the MoS_2 basal plane. The color code for atoms is yellow for S and greenish for Mo.

Table S3: The adsorption energies of hydrogen on 2Ti/S, 2Zr/S and 2Hf/S, without any correction (ΔG_E), with correction of H_2 energy which is our approximation (ΔG_H), with adding zero-point energy (ΔG_Z) and with the free energies of the different surfaces (ΔG_F).

	ΔG_E (eV)	ΔG_H (eV)	ΔG_Z (eV)	ΔG_F (eV)
2Ti/S	-0.27	-0.07	0.00	-0.16
2Zr/S	-0.11	0.09	0.17	-0.01
2Hf/S	-0.12	0.08	0.16	-0.02

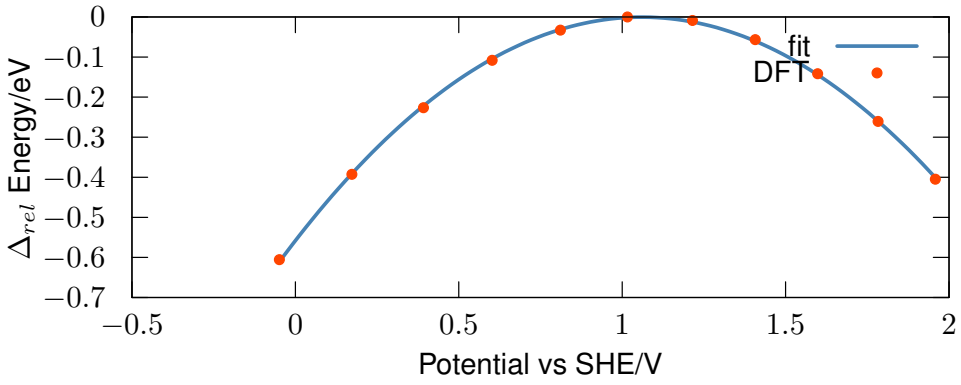

(a) Conductor

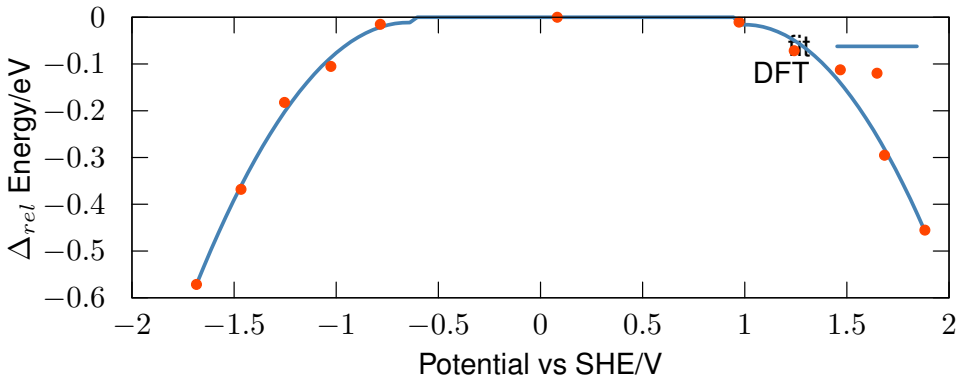

(b) Semi-conductor

Figure S4: Variation of the total energy as a function of the electrochemical potential (a) H@2Zr/S and (b) H@Mo/P with respect to the energy of the neutral slab.

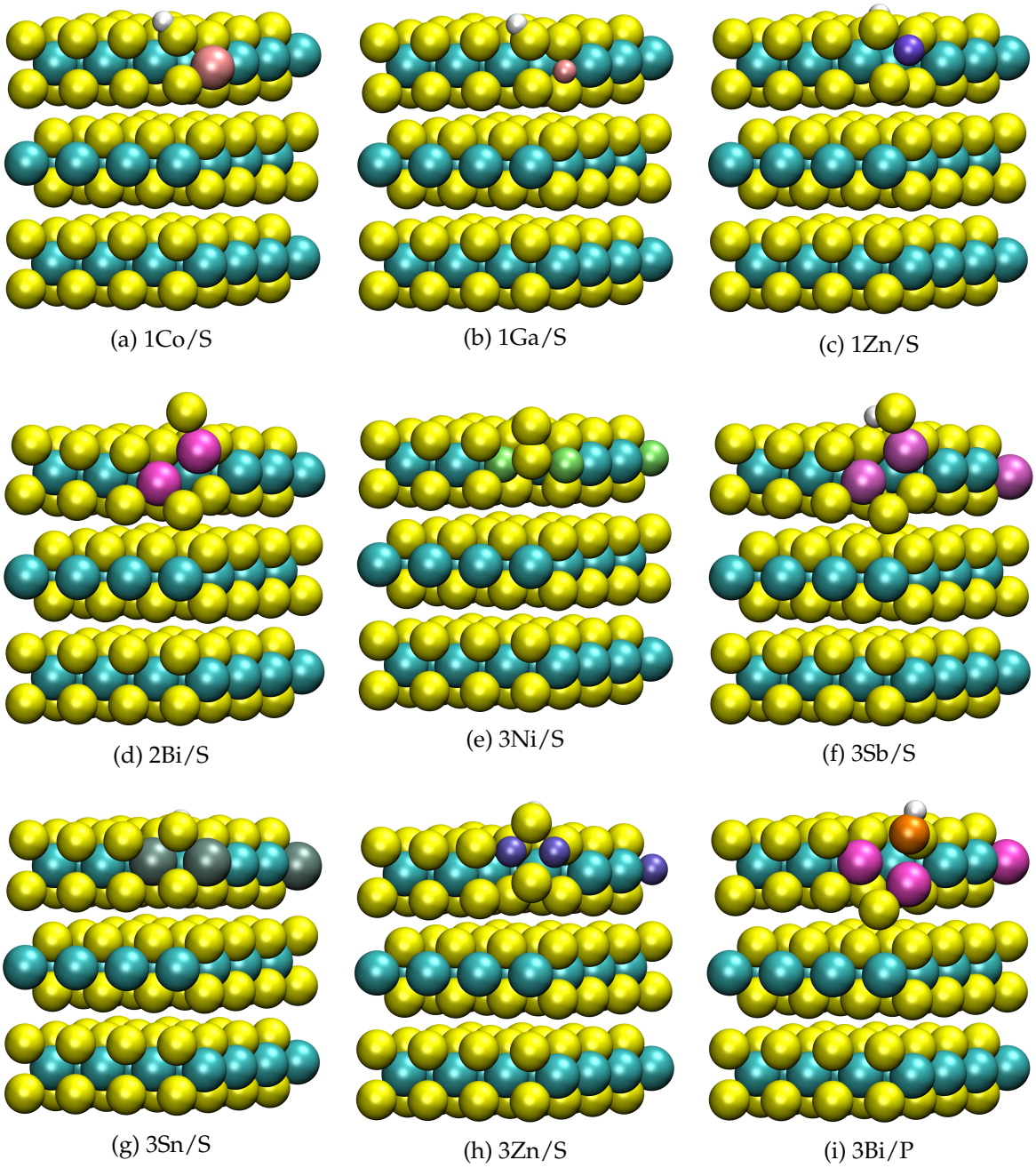

(a) 1Co/S (b) 1Ga/S (c) 1Zn/S

(d) 2Bi/S (e) 3Ni/S (f) 3Sb/S

(g) 3Sn/S (h) 3Zn/S (i) 3Bi/P

Figure S5: The different deformations of MoS_2 basal plane after the integration of many types of doping elements and the adsorption of hydrogen atom.

Table S4: The adsorption energies of hydrogen after the integration of different dopants to substitute Mo calculated with CHE method and before symmetrization

The doping elements	ΔG_H (eV)	The doping elements	ΔG_H (eV)
Ni		Cr	
3	-0.21	3	1.11
2	-0.50	2	1.11
1	-0.68	1	1.71
Co		Mn	
3	0.78	3	0.26
2	-0.63	2	0.94
1	-0.26	1	0.76
Fe		V	
3	0.87	3	-0.08
2	0.35	2	0.40
1	0.26	1	0.62
W		Zn	
3	2.11	3	-0.70
2	1.95	2	-0.57
1	1.91	1	-0.05
Zr		Nb	
3	0.17	3	0.09
2	0.09	2	0.56
1	0.52	1	0.69
Sn		Hf	
3	0.00	3	0.20
2	0.44	2	0.08
1	0.42	1	0.50
Ta		Sb	
3	0.24	3	-0.73
2	0.62	2	0.34
1	0.69	1	1.61
Bi		Ga	
3	-0.70	3	-0.73
2	-0.29	2	0.43
1	0.32	1	-0.30
Ti			
3	-0.12		
2	-0.07		
1	0.48		

Table S5: The adsorption energies of hydrogen after the integration of different dopants to substitute S calculated with CHE method and before symmetrization

The doping elements	ΔG_H (eV)
P	-0.71
O	1.14
Se	2.00
Te	1.90
N	-1.46

Table S6: The adsorption energies of hydrogen after the substitution of S by P and Mo by different dopants to substitute calculated with CHE method and before symmetrization

The doping elements of Mo	ΔG_H (eV)	The doping elements of Mo	ΔG_H (eV)
Ni		Cr	
3	0.45	3	-0.82
Co		Zr	
3	0.55	3	-0.41
Nb		Bi	
3	-1.01	3	0.21
2	-1.04	2	-0.50
1	-0.74	1	-0.48
Sn		Hf	
3	-0.26	3	-1.10
Ta		W	
3	-0.99	3	-0.67
Sb		Mn	
3	0.32	3	-0.03
Fe		Ga	
3	0.40	3	0.68

S3 Adsorption energy of H, OH and H_2O as a function of the potential

We analyse the typical evolution of ΔG_H(U), ΔG_{OH}(U), and ΔG_{H_2O}(U) as a function of electrochemical potential. As can be seen in Figure S6, ΔG_H(U) in eV decreases as one moves to more and more reducing electrochemical potentials with a slope close to unity, given that the Volmer reaction is a one-electron reduction step. OH* is not equivalent to the adsorption of formally charged OH^-. Rather, it is electrochemically formed via the reduction of H_2O, leading to a potential dependence very similar to the one of ΔG_H(U). Water adsorption, on the other hand, is formally a chemical step and, therefore, the adsorption energy of H_2O depends much less on the electrochemical potential compared to the adsorption of $H^+ + e^-$. This is the case for 3Ni/S (Figure S6a) and many other systems. Nevertheless, for some systems such as 3Sb/S (Figure S6b), the surface dipole moment of H_2O@MoS_2 leads to a very significant potential dependence due to its interaction with the potential-generated electric field.[S8] For water adsorption, this phenomenon is only observed when the surface features a significantly more pronounced geometrical distortion in the presence of the adsorbate compared to the pristine surface.

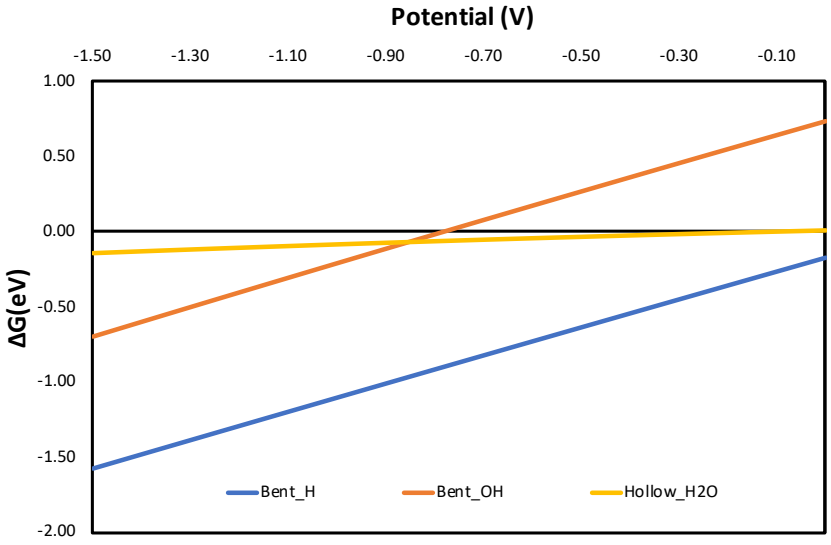

(a) 3Ni/S

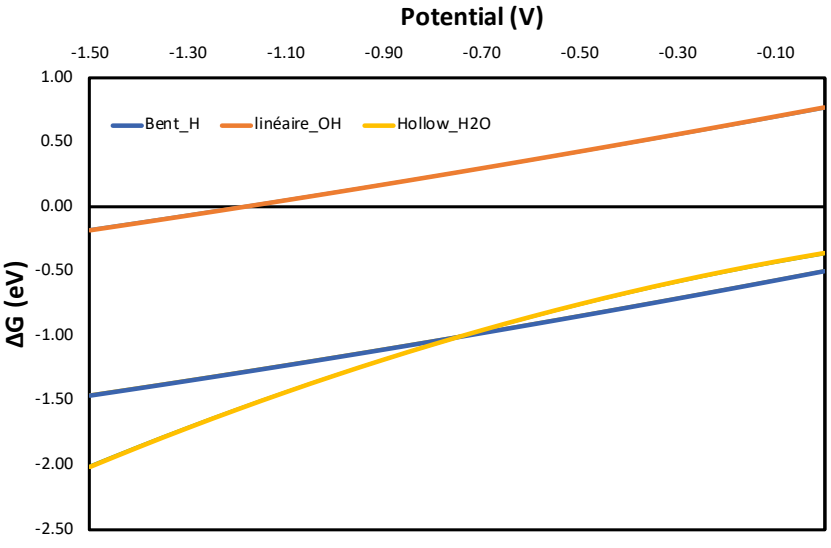

(b) 3Sb/S

Figure S6: Evolution of ΔG_H(U), ΔG_{OH}(U), and $\Delta G_{\mathrm{H_2O}}$(U) as a function of the electrochemical potential for two doped systems 3Ni/S and 3Sb/S.

S4 Density of states for selected systems

S5 Summary of Evaluation of Various Doped Systems

S6 Formation energy of Ti, Zr and Hf dimers

Table S7: The formation energy ΔE_f of Ti, Zr and Hf dimers.

Element	Mo_xS_{2x} (eV)	z Y (eV)	$Y_zMo_{x-z}S_{2x}$ (eV)	z Mo	ΔE_f (eV)
Ti	-1071.81	-16.08	-1066.07	-22.53	-0.7
Zr	-1071.81	-17.52	-1067.95	-22.53	-1.15
Hf	-1071.81	-20.57	-1071.10	-22.53	-1.25

S7 Dynamical stability of 2Ti/S, 2Zr/S and 2Hf/S

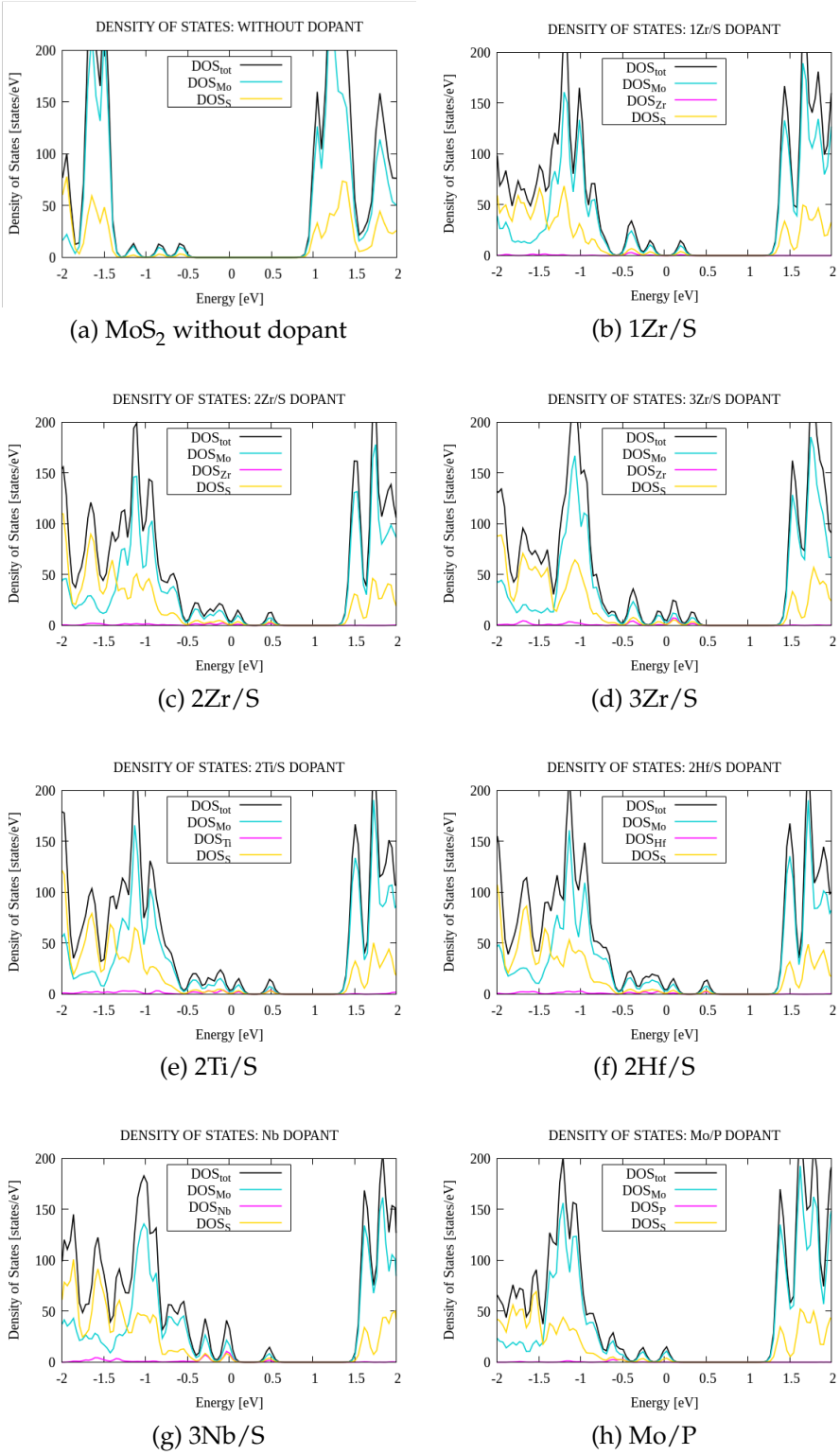

(a) MoS_2 without dopant

(b) 1Zr/S

(c) 2Zr/S

(d) 3Zr/S

(e) 2Ti/S

(f) 2Hf/S

(g) 3Nb/S

(h) Mo/P

Figure S7: Density of states of the perfect MoS_2 basal plane and with other different dopants.

	Dispersion	Cluster	Volmer (eV)	OH (eV)	Heyrovsky	Tafel	H2S release	Cycle OH/H2O (V)	Not just edge	Deformation	Conductivity /tau0[1/(ohm×m×s)]/10^16
3Ti/S +			-0.02	0.70							25.76
2Ti/S ++			0.08	0.87							22.72
3Ni/S +			-0.17	0.74							0.00
1Co/S			-0.29	0.61				0.4			12.29
3Mn/S											
1Fe/S			0.28	1.24							1.20
3V/S +			0.15	0.85							147.77
1V/S											
3Zn/S			-0.87	0.49							
1Zn/S			-0.02	0.82							34.43
3Nb/S											
1Nb/S											
3Zr/S +			0.29	1.28							37.56
2Zr/S ++			0.23	1.16							46.40
3Sn/S +			0.04	1.32							2.19
3Hf/S +			0.31	1.26							43.38
2Hf/S ++			0.26	1.17							62.80
3Sb/S			-0.50	0.77							
2Sb/S			0.23	1.54							0.15
3Bi/S +			-1.25	0.06				0.3			57.42
2Bi/S			-0.34	1.02							
1Bi/S											
1Ga/S			-0.16	0.81							26.75
3Ga/S			-0.73	0.68							
3Ta/S											
Mo/P			-0.33	-0.45				0.2			0.00
Mo/N			-1.20	0.99							
3Bi/P +			0.17	-0.29				0.5			2.15
3Nb/P			-0.97	-0.97		0.34					
2Nb/P			-0.79	-0.82		0.50					
1Nb/P			-0.68	-0.76		0.59		0.6			

Doping atoms are dispersed
Doping atoms are clusterized
Volmer Step is possible
OH is not adsorbed
Heyrovsky step is possible
Tafel Step is possible
H2S release is possible
Cycle OH/H2O is possible
Basal doping is possible
Doped surface is deformed
Conductivity of the promising systems

Figure S8: Summary of the results of the various tests carried out for each doped system. The cell colors are defined below the table. The values reported are at U(0V). For the first column, the systems in red are the active for HER and the systems with + are more promising than the others.

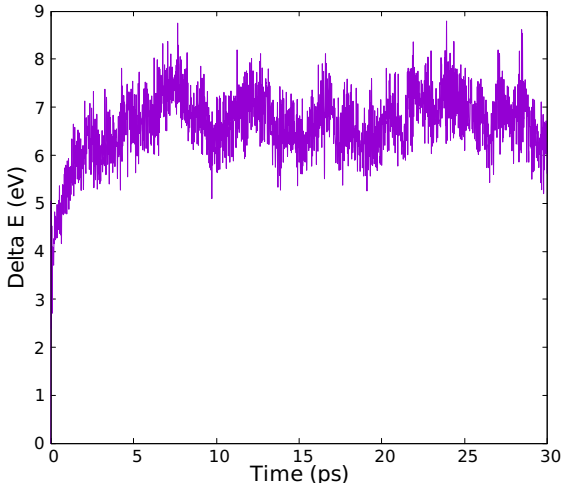

(a) 2Ti/S

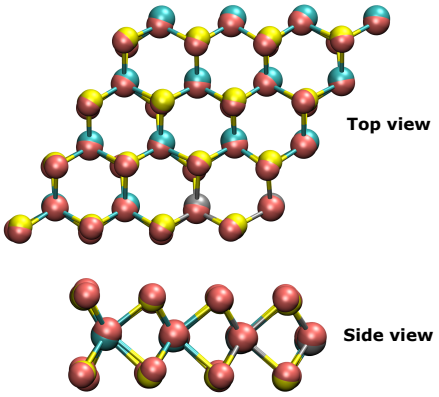

(b) 2Ti/S

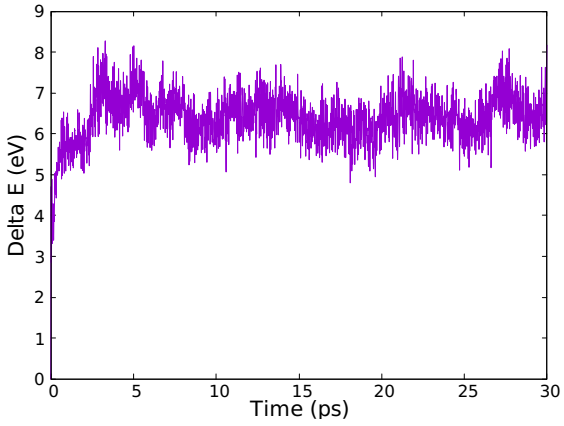

(c) 2Zr/S

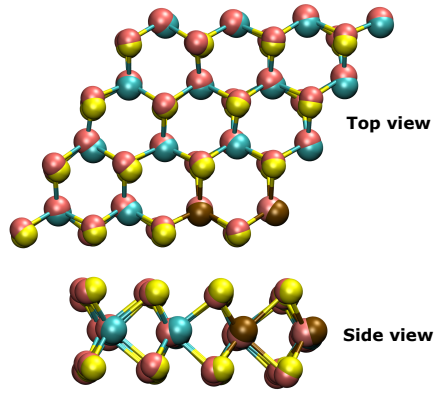

(d) 2Zr/S

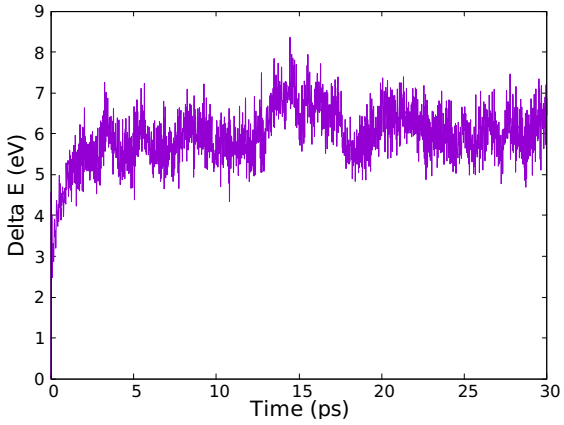

(e) 2Hf/S

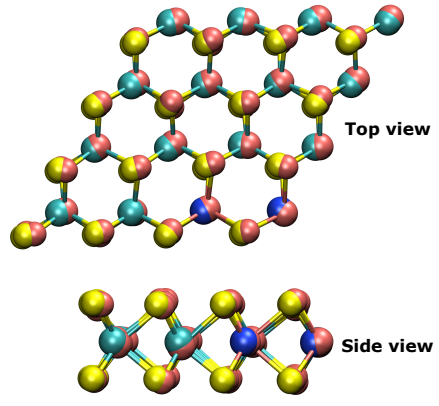

(f) 2Hf/S

Figure S9: (a), (c), (d) Evolution of the energy of the system as function of time: "Dynamical" stability of 2Ti, 2Zr and 2Hf/S systems by ab initio molecular dynamics calculations at 500 K and for 30 ps, (b), (d) and (f) Comparison between the structures at 0 ps and at 30 ps, the red color is for the new atom positions.

References

(S1) Remskar, M.; Mrzel, A.; Skraba, Z.; Jesih, A.; Ceh, M.; Demšar, J.; Stadelmann, P.; Lévy, F.; Mihailovic, D. Self-assembly of subnanometer-diameter single-wall MoS2 nanotubes. *Science* **2001**, *292*, 479–481.

(S2) Nath, M.; Govindaraj, A.; Rao, C. N. R. Simple synthesis of MoS2 and WS2 nanotubes. *Advanced Materials* **2001**, *13*, 283–286.

(S3) Lorenz, T.; Teich, D.; Joswig, J.-O.; Seifert, G. Theoretical study of the mechanical behavior of individual TiS2 and MoS2 nanotubes. *The Journal of Physical Chemistry C* **2012**, *116*, 11714–11721.

(S4) Chen, J.; Kuriyama, N.; Yuan, H.; Takeshita, H. T.; Sakai, T. Electrochemical hydrogen storage in MoS2 nanotubes. *Journal of the American Chemical Society* **2001**, *123*, 11813–11814.

(S5) Smidstrup, S.; Markussen, T.; Vancraeyveld, P.; Wellendorff, J.; Schneider, J.; Gunst, T.; Verstichel, B.; Stradi, D.; Khomyakov, P. A.; Vej-Hansen, U. G. et al. QuantumATK: An integrated platform of electronic and atomic-scale modelling tools. *J. Phys: Condens. Matter* **2020**, *32*, 015901.

(S6) Ansari, R.; Malakpour, S.; Faghihnasiri, M.; Sahmani, S. An ab initio investigation into the elastic, structural and electronic properties of MoS2 nanotubes. *Superlattices and Microstructures* **2015**, *82*, 188–200.

(S7) Colbeau-Justin, F.; Boissière, C.; Chaumonnot, A.; Bonduelle, A.; Sanchez, C. Aerosol Route to Highly Efficient (Co)Mo/SiO2 Mesoporous Catalysts. *Advanced Functional Materials* **2014**, *24*, 233–239.

(S8) Steinmann, S. N.; Sautet, P. Assessing a First-Principles Model of an Electrochemical

Interface by Comparison with Experiment. *The Journal of Physical Chemistry C* **2016**, *120*, 5619–5623.